TÜBİTAK

Turkish Journal of Chemistry

http://journals.tubitak.gov.tr/chem/

Research Article

Turk J Chem
(2017) 41: 760 – 772

doi:10.3906/kim-1701-9

Adsorption of Cu(II) on three adsorbents, Fe_3O_4/Ni/Ni_xB nanocomposite, carob (*Ceratonia siliqua*), and grape seeds: a comparative study

Tülin Deniz ÇİFTÇİ*
Department of Chemistry, Faculty of Science, Ege University, Bornova, İzmir, Turkey

Received: 02.01.2017 • **Accepted/Published Online:** 24.04.2017 • **Final Version:** 10.11.2017

Abstract: A novel adsorbent Fe_3O_4/Ni/Ni_xB nanocomposite was synthesized and used for the adsorption of copper. Moreover, natural adsorbents carob and grape seeds were used for this purpose. The surfaces and the elemental compositions of the adsorbents were characterized by SEM-EDX. The zero point charges of pH of Fe_3O_4/Ni/Ni_xB nanocomposite, carob, and grape seeds were found as 8.4, 6.0, and 5.6, respectively. The Langmuir, Freundlich, and Dubinin–Radushkevich isotherm models were used for the identification of the mechanism of the adsorption. The adsorptions of Cu(II) on the three adsorbents were well fitted to the Langmuir isotherm. The maximum adsorption capacities obtained from the Langmuir isotherm were 106.4, 15.6, and 15.9 mg/g for Fe_3O_4/Ni/Ni_xB nanocomposite, carob, and grape seeds, respectively. The equilibrium data of the isotherm models indicated that the Cu(II) adsorptions were favorable for all the adsorbents. The pseudo-first-order, pseudo-second-order, and Weber–Morris intraparticle diffusion models were used for the validation of the adsorption kinetics. The kinetic data were better fitted to the pseudo-second-order kinetic model for all the adsorbents. Fe_3O_4/Ni/Ni_xB nanocomposite, carob, and grape seeds are promising adsorbents for the adsorption of Cu(II) from water samples. The removal efficiencies were all about 100%.

Key words: Adsorption, carob, copper, Fe_3O_4/Ni/Ni_xB, grape seeds, nanocomposite

1. Introduction

It is well known that heavy metals are toxic to humans, animals, and plants. Environmental pollution has increased with the development of industry and manufacturing. Therefore, it has become necessary to develop new methods for the remediation of all the contaminants.

Copper is a transition metal and metallic copper is forgeable, flexible, and a good conductor of heat and electricity. It is usually found in compounds in the 2+ valence state but can also exist in metallic, 1+, and 3+ valence states. Volcanoes, forest fires, and sea spray are the natural sources of copper.[1] Copper smelters, foundries, and power stations are the anthropogenic activities leading to contamination by copper. Although it is an essential nutrient, it is also toxic for humans.[2] The toxicity of copper is called copperiedus. A metallic taste, vomiting, nausea, hypotension, and melena are some of the symptoms of acute copper poisoning by ingestion. Long-term (chronic) poisoning can result in damage of the liver and kidneys.[3] The World Health Organization reported a guidance value for copper in drinking water as 2 mg/L in 2003.[4] The same value was also reported in Turkey in 2005 by the Turkish Standards Institution (TS-266). Several methods such as precipitation, ion exchange, membrane filtration, electrolytic methods, and adsorption were used for the removal of contaminants.

*Correspondence: tulin.deniz.ciftci@ege.edu.tr

Low cost and simple maintenance make the adsorbents more attractive for removal. Various adsorbents such as γ-alumina support,[5] biosolids,[6] black tea waste,[7] cashew nut shells,[8] magnetic amidoximated chitosan-g poly(polyacrilonitrile)/laponite RD nanocomposites,[9] mansonia wood sawdust,[10] natural seed materials,[11] red mud,[12] and TEMPO-mediated oxidized cellulose nanofibrils modified PEI[13] were used for the adsorption of copper. Such adsorbents were also used for speciation of trace metals and metalloids based on their adsorptive properties[14]

This study presents the studies on the adsorption of Cu(II) on three different adsorbents. Fe_3O_4/Ni/Ni_xB nanocomposite**,** carob (*Ceratonia siliqua*), and grape seeds were used for this purpose. Fe_3O_4/Ni/Ni_xB nanocomposite is a novel adsorbent being used here for adsorption studies for the first time in the literature. Carob is a natural material and again used for the adsorption of Cu(II) for the first time. The zero point charge of the pH of the adsorbents, the effect of pH, and the adsorbent dose on the adsorption of Cu(II) were investigated. Isotherm and kinetic models were applied to the experimental data. Related constants and the adsorption capacities were determined. The results were compared with each other and some other adsorbents reported in the literature.

2. Results and discussion

Copper uptakes of the adsorbents were calculated using the following equation:

$$q = \frac{(C_i - C_e) \times V}{m} \tag{1}$$

where q is the Cu(II) uptake amount of the adsorbent (mg/g), C_i and C_e are the initial and the equilibrium concentrations of Cu(II) (mg/L), V is the volume of the Cu(II) solution (L), and m is the amount of the adsorbent (g).

2.1. Characterization

SEM images of the adsorbents were taken at various magnifications (Fe_3O_4/Ni/Ni_xB nanocomposite at 10,000×**,** carob (*Ceratonia siliqua*) at 2000×, and grape seeds at 2000× magnifications). Fe_3O_4/Ni/Ni_xB particles at nanoscale sizes are shown in Figure 1a. The porous structures of the carob and grape seeds are also shown in Figures 1b and 1c, respectively. EDX spectra of the adsorbents showed that the element compositions (mass %) are Fe 40.8, Ni 29.1, O 26.9, B 3.2% for Fe_3O_4/Ni/Ni_xB; C 95.9, Ca 1.8, Mo 1.1, K 0.8, Mg 0.4% for carob; and C 96.1, Ca 1.8, K 1.1, Mo 0.6, P 0.3, Mg 0.1, Al 0.1% for grape seeds. The magnetic property of the Fe_3O_4/Ni/Ni_xB nanocomposite is shown in Figure 1d. The nanoparticles can be separated from the solution by a magnet.

2.2. Zero point charge of pH

Determination of the pH_{PZC} of an adsorbent is very important for adsorption studies. Below the pH_{PZC}, the surface of the adsorbent is positively charged. At higher pH levels than the pH_{PZC}, the surface is then negatively charged.

Either 0.1 mol/L HNO_3 or NaOH solution was added to 0.1 mol/L $NaNO_3$ solution in order to adjust the pH. Solutions with pH levels from 2 to 12 were added to the adsorbents to determine the pH_{PZC} of the adsorbents. The suspensions were shaken for 24 h. The equilibrium pH levels were measured and ΔpH values were calculated. The graph of ΔpH versus the initial pH is shown in Figure 2. As shown in Figure 2, the zero

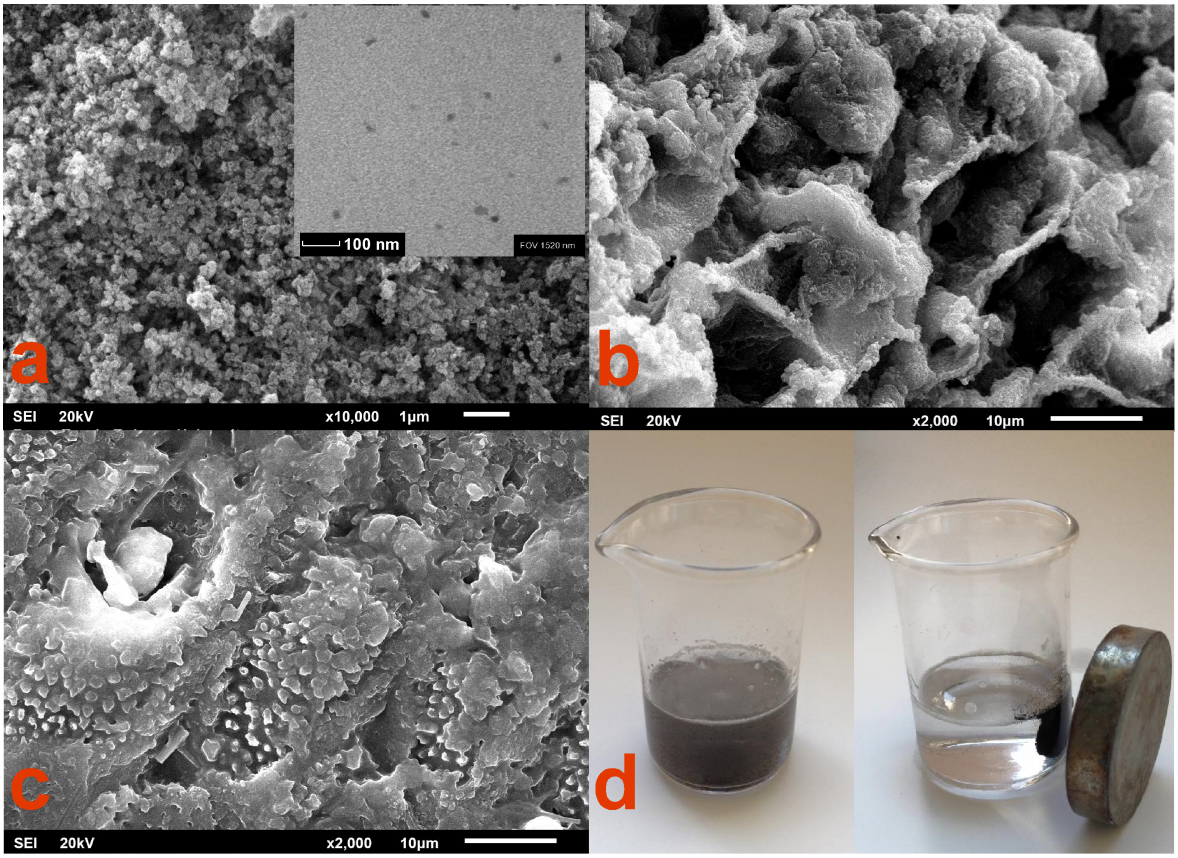

Figure 1. SEM images of the materials used in the study for the adsorption of Cu(II): a) Fe_3O_4/Ni/Ni_xB nanocomposite at 10,000× magnification (insert shows TEM image of the nanoparticles), b) carob at 2000× magnification, c) grape seeds at 2000× magnification, d) separation of Fe_3O_4/Ni/Ni_xB nanocomposite from the solution by a magnet.

point charge of pH values was determined as 8.4, 6.0, and 5.6 for the nanoparticles, carob, and grape seeds, respectively.

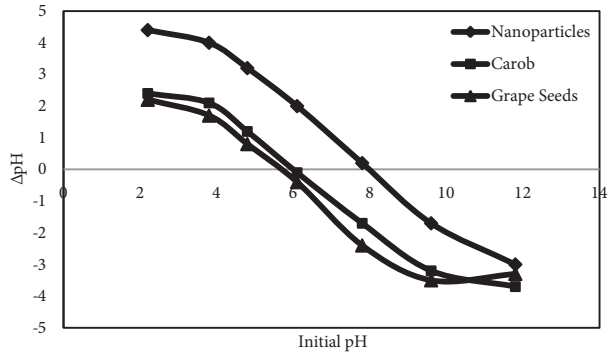

Figure 2. Zero point charge of pH of the adsorbents (pH range: 2–12; adsorbents: 0.1 g; solution: 25 mL of 0.1 mol/L $NaNO_3$; shaken at 25 °C for 24 h).

2.3. Effect of pH

The pH of the solution plays an important role for the adsorption processes. The ionization and the specification of the adsorbate and the charge of the surface of the adsorbent were affected by the pH of the solution [12] Cu(II) uptakes of the adsorbents against the initial pH are shown in Figure 3. It was calculated from the solubility product constant of $Cu(OH)_2$ ($K_{sp} = 2 \times 10^{-19}$) that the precipitation starts at about pH 6.5. While preparing the solutions at different pH levels, $Cu(OH)_2$ precipitates at higher pH levels than 6.5 as already seen. Since increasing the pH causes a decline in adsorption due to the formation of $Cu(OH)_2$ precipitate, although the maximum Cu(II) uptakes were observed at about pH 8 and 10 for carob and grape seeds, respectively, pH 5.5 was chosen for further studies. Similar results were reported by Al-Qodah et al., [15] Nadaroglu et al., [12] and SenthilKumar et al. [8]

The graph for the Fe_3O_4/Ni/Ni_xB nanocomposite is different from the others. Cu(II) uptakes remained at the same level for all the pH levels studied. Again, pH 5.5 was chosen for further studies for the same reason.

2.4. Effect of adsorbent dose

The adsorption study was done with various amounts of the adsorbents. The adsorbent doses ranged from 0.2 to 20 g/L. As shown in Figure 4, removal efficiencies increased with the adsorbent dose for all the adsorbents. This can be explained by the increasing of the surface area and the adsorption site numbers. The adsorbent dose of 4.0 g/L was chosen for carob and grape seeds and the adsorbent dose of 2.0 g/L was chosen for the Fe_3O_4/Ni/Ni_xB nanocomposite for further studies.

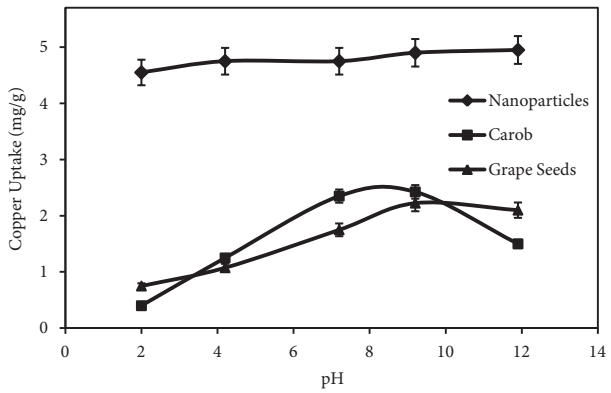

Figure 3. Effect of pH on the Cu(II) uptakes of the adsorbents (pH range: 2–12; adsorbents: 0.05 g Fe_3O_4/Ni/Ni_xB nanocomposite, 0.1 g carob, 0.1 g grape seeds; solution: 25 mL of 10 mg/L Cu(II); adsorption at 25 °C for 24 h). The error bars represent the standard deviations of three measurements.

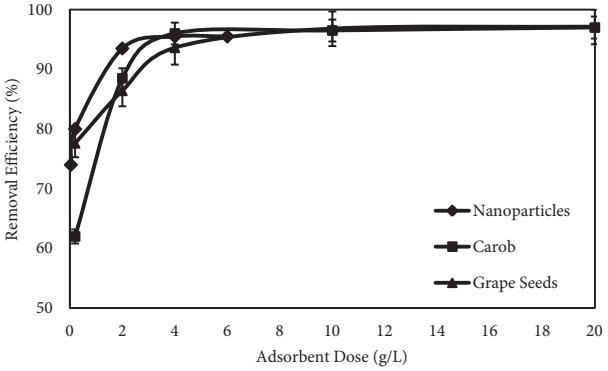

Figure 4. Effect of adsorbent dose on the removal efficiencies of the adsorbents (pH 5.5; adsorbents: 0.005–0.5 g; solution: 25 mL of 10 mg/L Cu(II); adsorption at 25 °C for 24 h). The error bars represent the standard deviations of three measurements.

2.5. Isotherm studies

The Langmuir, [16] Freundlich, [17] and Dubinin–Radushkevich (D-R) [18] isotherm models (Table 1) are the most commonly used isotherms for the identification of the mechanism of the adsorption and the relation between the amount of the adsorbate in the liquid and solid phases at equilibrium. The Langmuir isotherm model describes a monolayer adsorption on a homogeneous surface, whereas the Freundlich isotherm model is used for

Table 1. Isotherm parameters of Cu(II) adsorption on the adsorbents.

Isotherm model	Parameter	Fe_3O_4/Ni/Ni_xB nanocomposite	Carob	Grape seeds
Langmuir isotherm $q_e = \frac{q_m K_L C_e}{1+K_L C_e}$ $R_L = \frac{1}{1+K_L C_0}$	Equation	$q_e = \frac{7.22C_e}{1+0.068C_e}$	$q_e = \frac{0.41C_e}{1+0.026C_e}$	$q_e = \frac{0.10C_e}{1+0.0062C_e}$
	q_m (mg/g)	106.4	15.6	15.9
	K_L (L/mg)	0.068	0.026	0.0062
	R^2	0.9967	0.9954	0.9952
	Separation factor	0.03–0.88	0.07–0.95	0.24–0.99
Freundlich isotherm $q_e = K_F C_e^{\frac{1}{n}}$	Equation	$q_e = 6.4C_e^{0.64}$	$q_e = 1.0C_e^{0.48}$	$q_e = 0.27C_e^{0.70}$
	K_F (mg/g)	6.4	1.0	0.21
	n	1.55	2.08	1.44
	R^2	0.8879	0.9808	0.9492
D-R isotherm $\ln Q = -k\varepsilon^2 + lnQ_m$ $E = \frac{1}{\sqrt{-2k}}$	Equation	$\ln Q = -0.0058\varepsilon^2 - 4.72$	$\ln Q = -0.0059\varepsilon^2 - 7.21$	$\ln Q = -0.0071\varepsilon^2 - 7.46$
	Q_m (mol/g)	8.9×10^{-3}	7.4×10^{-4}	5.7×10^{-4}
	k (mol^2/kJ^2)	0.0058	0.0059	0.0071
	E (kJ/mol)	9.3	9.2	8.4
	R^2	0.9434	0.9844	0.9446

the description of the adsorption on heterogeneous surfaces and active sites with different energies. The D-R model is used for the identification of the nature of the adsorption.

The isotherm graphs for the Langmuir, Freundlich, and D-R models are shown in Figures 5a, 5b, and 5c, respectively. The constants and the regression coefficients are listed in Table 1. According to the regression coefficient (R^2) values obtained, the adsorption data of Cu(II) on the Fe_3O_4/Ni/Ni_xB nanocomposite, carob, and grape seeds were better fitted to the Langmuir isotherm, meaning that the monolayer adsorption occurred on a homogeneous surface. The maximum adsorption capacities of the adsorbents were 106.4, 15.6, and 15.9 mg/g for the Fe_3O_4/Ni/Ni_xB nanocomposite, carob, and grape seeds, respectively. All the separation factor (R_L) values obtained from the Langmuir isotherm ranged from 0.1 to 1, meaning that the adsorption of Cu(II) on the three adsorbents was favorable. The values of n obtained from the Freundlich isotherm were greater than 1, which also indicated that the adsorptions of Cu(II) on all the adsorbents were favorable.

The mean sorption energy, E, which is defined as the free energy required for the transfer of 1 mol solute from infinity to the surface of the adsorbent, was calculated from the D-R isotherm to be 9.3, 9.2, and 8.4 kJ/mol for the adsorption of Cu(II) on the nanoparticles, carob, and grape seeds, respectively, which suggests that the adsorption processes may be driven by a chemical ion exchange mechanism.[18]

2.6. Kinetic studies

The pseudo-first-order (PFO),[19] pseudo-second-order (PSO),[20] and Weber–Morris intraparticle diffusion[21] models (Table 2) were used for the validation of the adsorption kinetics. As shown in Figure 6a, the adsorption rates of the Cu(II) with the nanoparticles, carob, and grape seeds were rapid during the first 5, 20, and 20 min, respectively. However, in the second stage, the adsorption rate was much lower because of the decreasing of the active sites. The PSO model is based on the assumption that the rate-limiting step is chemical adsorption or chemisorptions involving valence forces through sharing or exchange of electrons between the adsorbent and adsorbate as covalent forces.[9] The Weber–Morris intraparticle diffusion model was also used for verifying the influence of mass resistance on the binding of Cu(II) on the adsorbents.

Table 2. Kinetic parameters of Cu(II) adsorption on the adsorbents.

Kinetic Model	Parameter	Fe_3O_4/Ni/Ni_xB nanocomposite	Carob	Grape seeds
Pseudo-first-order $\log(q_e - q_t) = \log q_e - \frac{k_1}{2.303}t$	Equation	$\log(0.36 - q_t) = -0.002t - 0.4389$	$\log(1.36 - q_t) = -0.0026t + 0.1323$	$\log(1.55 - q_t) = -0.0023t + 0.1905$
	q_e (mg/g)	0.36	1.36	1.55
	k_1 (L/min)	4.6×10^{-3}	6.0×10^{-3}	5.3×10^{-3}
	R^2	0.8609	0.8680	0.7219
Pseudo-second-order $\frac{t}{q_t} = \frac{1}{h} + \frac{1}{q_e}t$	Equation	$\frac{t}{q_t} = 0.1995t + 0.65$	$\frac{t}{q_t} = 0.3918t + 11.09$	$\frac{t}{q_t} = 0.3880t + 16.07$
	q_e (mg/g)	5.01	2.55	2.58
	k_2 (g/mg min)	0.061	0.014	0.009
	R^2	1	0.9993	0.9989
Intraparticle diffusion $q_t = k_{int}t^{0.5} + I$	Equation	$q_t = 0.0105t^{0.5} + 4.65$	$q_t = 0.0387t^{0.5} + 1.23$	$q_t = 0.0469t^{0.5} + 0.97$
	I (mg/g)	4.65	1.23	0.97
	k_{int} (mg/g $\min^{0.5}$)	0.0105	0.0387	0.0469
	R^2	0.9232	0.8054	0.7502

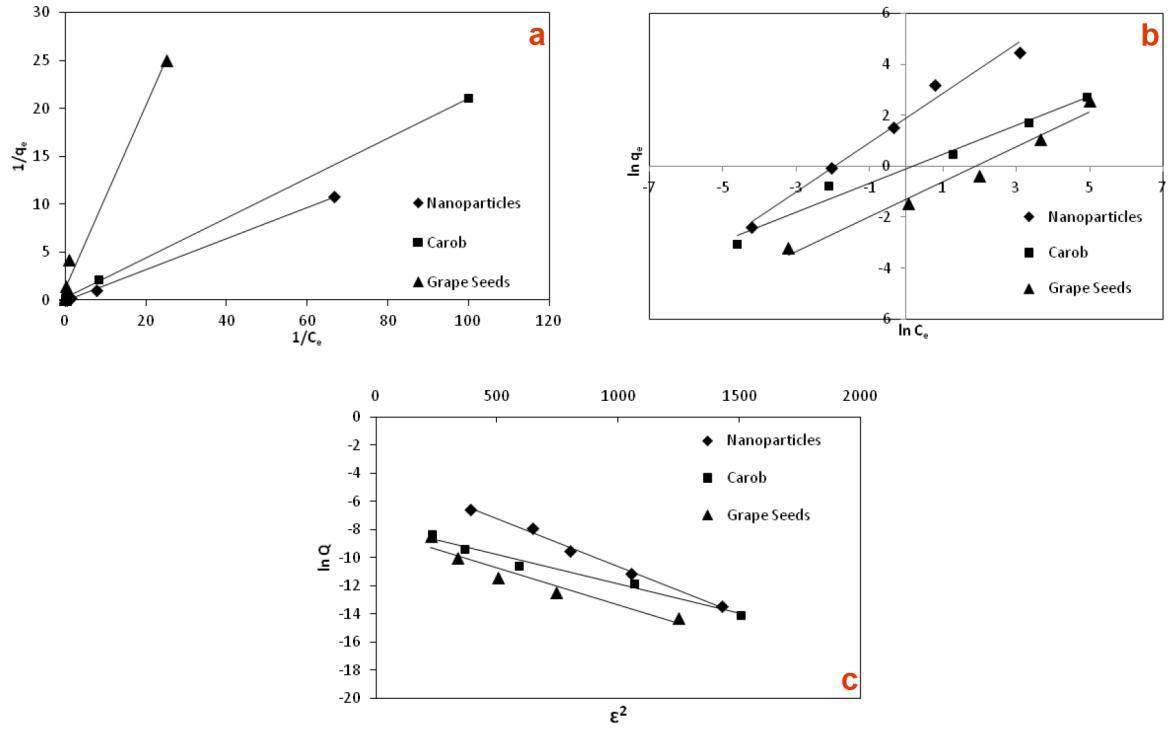

Figure 5. Isotherm graphs for the adsorption of Cu(II) on the adsorbents: a) Langmuir isotherm, b) Freundlich isotherm, c) D-R isotherm (pH 5.5; adsorbents: 0.05 g Fe_3O_4/Ni/Ni_xB nanocomposite, 0.1 g carob, 0.1 g grape seeds; solution: 25 mL of 0.2–200 mg/L Cu(II); adsorption at 25 °C for 24 h).

The PFO kinetic plots for the adsorption of Cu(II) on the adsorbents are shown in Figure 6b. Theoretical values of q_e and the first-order rate constant (k_1) were calculated from the slope and the intercept and are shown in Table 2. The theoretical values of q_e for the adsorption of Cu(II) on the nanoparticles (0.36 mg/g), carob (1.36 mg/g), and grape seeds (1.55 mg/g) are low as compared with the experimental values of 5.0 mg/g, 2.5 mg/g, and 2.5 mg/g, respectively, which indicates that the adsorption of Cu(II) on all the adsorbents did not follow the PFO kinetic model. The highest regression coefficients were obtained with the PSO kinetic model (Figure 6c) as compared with the other kinetic models, which indicated that chemisorptions played a dominant role. Moreover, the theoretical values of q_e for the adsorption on the nanoparticles (5.01 mg/g), carob (2.55 mg/g), and grape seeds (2.58 mg/g) are very close to 5.0 mg/g, 2.5 mg/g, and 2.5 mg/g, which are the experimental values.

If intraparticle diffusion is assumed to be the sole rate-controlling step, the plot passes through the origin.[23] However, the plot for all the adsorbent did not pass through the origin. Three stages were observed for the adsorption of Cu(II) on the adsorbents carob and grape seed (Figure 6d). In the first and second stages, the adsorption occurs on the external surface (external diffusion) and the inner sites of the adsorbent (intraparticle diffusion), respectively. The ions were diffused to the smaller pores of the adsorbent in the last stage (plateau to equilibrium).

2.7. Application to real samples

Column systems are preferred for small-scale treatment technologies for their simple and fast application. Certified reference material (EP-L-2), tap water, and waste water were used for the application to real samples.

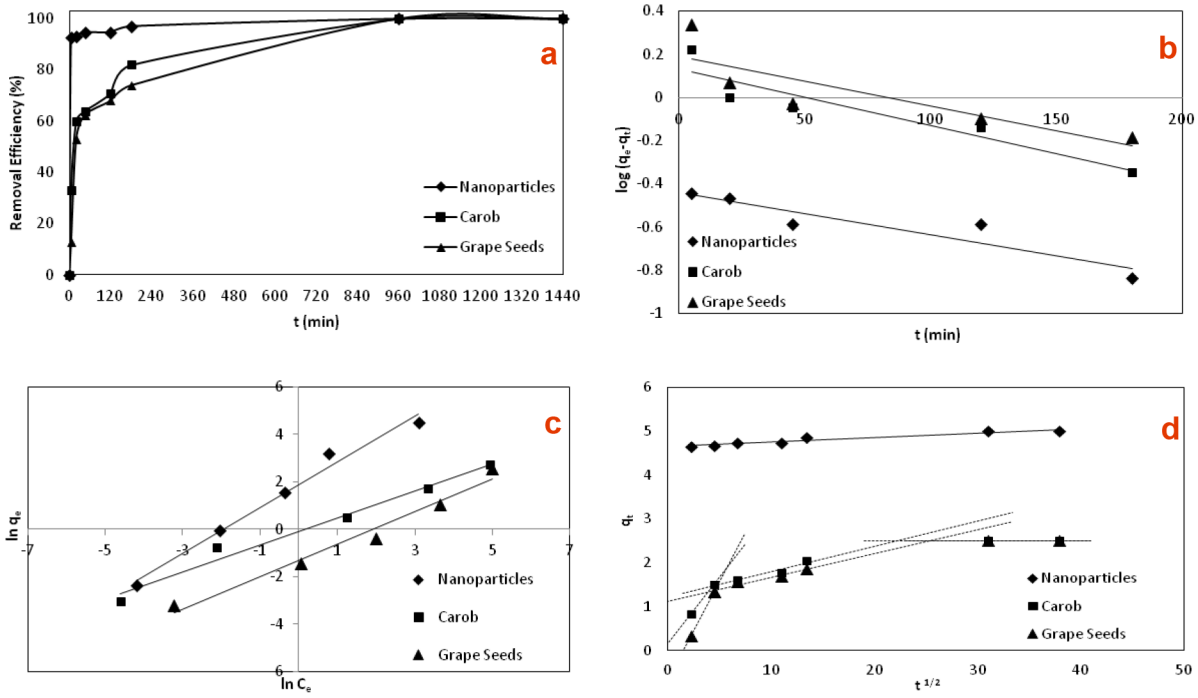

Figure 6. Kinetic model graphs for the adsorption of Cu(II) on the adsorbents: a) Cu(II) uptake values versus time, b) pseudo-first-order (PFO), c) pseudo-second-order (PSO), d) Weber–Morris intraparticle diffusion (pH 5.5; adsorbents: 0.05 g Fe_3O_4/Ni/Ni_xB nanocomposite, 0.1 g carob, 0.1 g grape seeds; solution: 25 mL of 10 mg/L Cu(II); adsorption at 25 °C for 5–1440 min).

The concentrations of Cu(II) in real sample water were determined with flame AAS. The Cu(II) concentration in EP-L-2 was 16.2 ± 0.3 mg/L, in tap water was <0.01 mg/L (below the limit of detection), and in waste water was 0.20 ± 0.01 mg/L. The concentration of Cu(II) after the adsorption in the certified reference material (EP-L-2, drinking water) was below the limit of detection. The removal efficiency was calculated to be >99.9%. Since the concentrations of Cu(II) in the tap water and the waste water samples were low, Cu(II) spiking at different concentrations was done. After the adsorption, the values obtained by the three adsorbents were found as listed in Table 3.

2.8. Comparison with the other adsorbents

The adsorbents used for the adsorption of Cu(II) and reported in the literature were compared with the Fe_3O_4/Ni/Ni_xB nanocomposite, carob, and grape seeds. As shown in Table 4, the maximum adsorption capacity of the Fe_3O_4/Ni/Ni_xB nanocomposite was much higher than the other adsorbents compared (except that of one previous study).[9] The maximum adsorption capacities of the carob and grape seeds were also close to those of natural seed materials and cashew nut shells. The equilibrium data of most of the adsorbents better fitted to the Langmuir isotherm. Similarly, the kinetic data were better fitted to the PSO model.

3. Conclusion

The adsorptions of Cu(II) on Fe_3O_4/Ni/Ni_xB nanocomposite, carob, and grape seeds were reported and compared for the first time in the literature. The zero point charges of the pH of the Fe_3O_4/Ni/Ni_xB nanocom-

Table 3. Application to real samples.

		Tap water		Waste water	
Adsorbent	Spiked Cu(II) (mg/L)	Cu(II) after the adsorption (mg/L)	Removal efficiency (%)	Cu(II) after the adsorption (mg/L)	Removal efficiency (%)
Fe_3O_4/Ni/Ni_xB					
	0	BLD	*	BLD	> 99.0
	1	BLD	> 99.0	0.14	88.3
	10	0.02	99.8	0.74	92.7
	100	0.06	99.9	0.38	99.6
Carob					
	0	BLD	*	BLD	> 99.0
	1	0.02	98.0	0.17	85.8
	10	BLD	> 99.9	0.50	95.1
	100	0.04	100.0	0.48	99.5
Grape Seed					
	0	BLD	*	BLD	> 99.0
	1	0.03	97.0	0.20	83.3
	10	0.04	99.6	1.35	86.8
	100	0.14	99.9	3.20	96.8

*: Since the concentration of copper in tap water was below the limit of detection, the removal efficiency (for zero spike addition) was not calculated.
Before the adsorption, the concentrations of copper in tap water and waste water were BLD and 0.2 mg/L, respectively.
BLD: Below the limit of detection, i.e. 0.01 mg/L.

Table 4. Comparison of the maximum Cu(II) adsorption capacities with the other reported adsorbents.

Adsorbent	Initial concentration (mg/L)	Capacity (mg/g)	Isotherm model	Kinetic model Kinetic model	Reference
Magnetic chitosan-g-poly-acrylonitrile/laponite RD	25–1000	533	Langmuir	PSO	[9]
Fe_3O_4/Ni/Ni_xB	0.2–200	106.4	Langmuir	PSO	This study
Chitosan ligand	50	88.07	Langmuir	PSO	[25]
Green algal biomass	40–400	65	Langmuir	PSO	[15]
TEMPO-mediated oxidized cellulose nanofibrils modified PEI	1–300	52.32	Langmuir	PSO	[13]
Black tea waste	25.4	43.18	Langmuir	PSO	[7]
Mansonia wood sawdust	60–140	42.37	Langmuir	-	[10]
Cashew nut shell	10–50	20.00	Langmuir/Freundlich	PSO	[8]
Grape seeds	0.2–200	15.9	Langmuir	PSO	This study
Carob	0.2–200	15.6	Langmuir	PSO	This study
Natural seed materials	100	13.14	Langmuir/Freundlich	-	[11]
Red mud	190.5	5.35	Langmuir	-	[12]

posite, carob, and grape seeds were found to be 8.4, 6.0, and 5.6, respectively. The optimum adsorbent doses were determined as 4.0 g/L for carob and grape seeds and 2.0 g/L for the Fe_3O_4/Ni/Ni_xB nanocomposite. Equilibrium studies showed that the Cu(II) adsorptions on the three adsorbents were well fitted to the

Langmuir isotherm. The model suggested that monolayer adsorption occurred on a homogeneous layer. The maximum adsorption capacities obtained from the Langmuir isotherm were 106.4, 15.6, and 15.9 mg/g for the Fe_3O_4/Ni/Ni$_x$B nanocomposite, carob, and grape seeds, respectively. Although carob and grape seeds are cheap adsorbents, their capacities were low. The coefficients calculated from the Langmuir and the Freundlich isotherms indicated that the Cu(II) adsorptions were favorable for all the adsorbents. The D-R isotherm showed that the adsorption processes were driven by the chemical ion exchange mechanism. The kinetic data were better fitted to the PSO kinetic model for all the adsorbents, which indicated that chemisorptions played a dominant role. The adsorption study was successfully applied to real water samples. The removal efficiencies were all about 100%.

4. Experimental

4.1. Materials

Ultrapure water was used for all the experiments (GenPure, TKA, Germany). All the reagents used in the experiments were of analytical grade. First, 1000 mg/L of stock Cu(II) solution was prepared from $CuSO_4.5H_2O$ (Merck, Germany) in 1% HNO_3 solution. More diluted solutions were prepared daily just before the experiments. $FeCl_2.4H_2O$ (Merck), $FeCl_3.6H_2O$ (Merck), and $NiSO_4.6H_2O$ (Merck) were used for the preparation of Fe_3O_4/Ni/Ni$_x$B nanocomposite adsorbent. Solutions of NaOH, HCl, and HNO_3 were used for pH adjustments and prepared from NaOH (Merck), HCl (Merck), and HNO_3 (Merck), respectively.

4.2. Equipment

A Varian 220 FS model flame atomic absorption spectrometer (324.7 nm wavelength, 0.5 nm slit width, air-acetylene flame) was used for the analysis of Cu(II). The limit of detection of the analysis of copper was 0.01 mg/L, which was calculated as three times the standard deviation of the blank solution. The limit of quantification of the analysis of copper was 0.03 mg/L, which was calculated as ten times the standard deviation of the blank solution. Characterization of the adsorbents was performed using a JEOL JSM-6610 model scanning electron microscopy combined with energy dispersive X-ray spectroscopy (SEM-EDX) and a Delong Instruments LVEM5 model transmission electron microscopy (TEM). A Mettler Toledo FG2 model pH meter was used for the determination of pH. Buffer solutions at pH 4, 7, and 10 were used for the calibration of the pH meter before use. A Biosan OS-10 model shaker with a water bath was used for the batch experiments at a fixed temperature. All the experiments were done in at least duplicate.

4.3. Preparation of the adsorbents

4.3.1. Fe_3O_4/Ni/Ni$_x$B nanocomposite

A preparation method similar to that for Ni/Ni$_x$B[24] was used for the preparation of the Fe_3O_4/Ni/Ni$_x$B nanocomposite. Appropriate amounts of $FeCl_2.4H_2O$ (0.1 mol), $FeCl_3.6H_2O$ (0.2 mol), and $NiSO_4.6H_2O$ (0.1 mol) were weighed and placed in a beaker, and 2.5 mL of 1 mol/L HCl and the required amount of distilled water were added for dissolving the solid. The solution was then diluted to 250 mL and 25 mL of 36% $NaBH_4$ was added to the solution drop by drop. After gas evolution ceased, black nanoparticles were washed thoroughly with distilled water and then acetone. The solid was then dried in an oven at 70 °C.

4.3.2. Carob and grape seeds

Carob and grape seeds were purchased from a herbal market. The seeds of the carob were removed. The carob and the grape seeds were ground separately. The size of the particles was adjusted to a range of 0.250–0.355 mm by a mesh sieve. The particles were then thoroughly washed with distilled water to remove impurities and soluble materials. The carob and grape seeds were dried in an oven at 70 °C for 24 h.

4.4. Characterization

The adsorbents were characterized by SEM-EDX. The surface structure was mapped using SEM at various magnifications. Element mapping was also done by EDX. The nanosize of the nanocomposite was also determined by TEM.

4.5. Adsorption studies

Zero point charge of pH, effect of pH, and effect of adsorbent dose studies were done. Batch experiments were used for the identification of the relation of the adsorbate and adsorbents. Unless otherwise stated, the adsorption study was done with 0.05 g of nanoparticles and 0.1 g of carob and 0.1 g of grape seeds. The adsorbents were placed in a Falcon tube (50 mL volume) and 25 mL of 10 mg/L Cu(II) solution at pH 5.5 was added to the mixtures and shaken at 25 °C for 24 h. Carob and grape seed adsorbents were separated from the solution by filtrating with black band filter paper. Since the Fe_3O_4/Ni/Ni_xB nanocomposite had a magnetic property, nanoparticles were separated from the solution by a magnet. The remaining Cu(II) in the solution was determined by flame atomic absorption spectrometer.

4.6. Zero point charge of pH

Either 0.1 mol/L HNO_3 or NaOH solution was added to the 0.1 mol/L $NaNO_3$ solution for adjusting the pH. The pH levels of the solutions ranged from 2 to 12. Next, 25 mL of solution was added to 0.1 g of adsorbents and shaken at 25 °C, and 24 h later, the pH of the supernatant solutions was measured.

4.7. Effect of pH

First, 10 mg/L Cu(II) solutions were prepared at different pH levels by the addition of either HCl or NaOH. The solutions were added to the adsorbents and shaken at 25 °C for 24 h. Carob and grape seeds were separated from the solution by filter paper and Fe_3O_4/Ni/Ni_xB nanoparticles were separated by a magnet. The remaining Cu(II) in the solutions was determined.

4.8. Effect of adsorbent dose

Adsorbent was weighed in amounts of 0.005, 0.05, 0.1, 0.25, and 0.5 g and 25 mL of 10 mg/L Cu(II) solution at pH 5.5 was added to the adsorbents and shaken at 25 °C for 24 h. The adsorbents were separated from the solutions as described earlier and the solutions were analyzed.

4.9. Isotherm studies

First, 25 mL of Cu(II) solutions at various concentrations (0.2, 2, 10, 50, and 200 mg/L) at pH 5.5 was added to the adsorbents and shaken at 25 °C, and 24 h later, the adsorbents were separated from the mixture as described earlier and the solution was analyzed. The experimental data were fitted to the Langmuir, Freundlich, and D-R isotherm models.

4.10. Kinetic studies

The PFO, PSO, and Weber–Morris intraparticle diffusion models were used for the adsorption kinetics. First, 25 mL of 10 mg/L Cu(II) solution at pH 5.5 was added to the adsorbents and shaken at 25 °C for various times (5, 20, 45, 120, 180, and 1440 min). The adsorbents were separated from the mixture as described earlier and the remaining Cu(II) was determined. The experimental data were fitted to the kinetic models (Table 2).

4.11. Application to real samples

Column experiments were also done for the application to real samples. The adsorption method was applied to the certified reference material (EnviroMAT Drinking Water-Low, EP-L-2), tap water (pH 7.6), and waste water (pH 7.9) samples using a glass column of 30 cm in length and 1.0 cm in diameter. Glass wool was placed at the bottom of the columns and 0.2 g of nanocomposite and 1.0 g of carob and grape seeds were filled into the columns. Again, glass wool was placed at the top of the columns. Water samples and 1, 10, and 100 mg/L of Cu(II)-spiked water samples were passed through the columns at 3 mL/min flow rate and the remaining Cu(II) was determined.

Acknowledgments

I acknowledge the Boğaziçi University Center for Life Sciences and Technologies for TEM experiments. I would also like to thank high school students Tibet Çiğdem and Atilla Selim Dinç and their teacher, Serpil Yapıcı, for their kind help during laboratory studies.

References

1. Battersby, S. *Clay's Handbook of Environmental Health*, 20th ed.; E & FN Spon: New York, NY, USA, 2011.
2. Friis, R. H. *Essentials of Environmental Health*, 2nd ed.; Jones and Bartlett Learning: Sudbury, MA, USA, 2012.
3. World Health Organization. Copper in Drinking-Water Background Document for Development of WHO Guidelines for Drinking-Water Quality. WHO: Geneva, Switzerland, 2011.
4. World Health Organization. *Guidelines for Drinking-Water Quality*, 4th ed.; WHO: Geneva, Switzerland, 2011.
5. Papas, B. N.; Whitten, J. L. *Surf. Sci.* **2016**, *651*, 22-27.
6. Sarioglu, M.; Güler, U. A.; Beyazit, N. *Desalination* **2009**, *239*, 167-174.
7. Weng, C. H.; Lin Y. T.; Hong, D. Y.; Sharma, Y. C.; Chen, S. C.; Tripathi, K. *Ecol. Eng.* **2014**, *67*, 127-133.
8. SenthilKumar, P.; Ramalingam, S.; Sathyaselvabala, V.; Kirupha, S. D.; Sivanesan, S. *Desalination* **2011**, *266*, 63-71.
9. Mahdavinia, G. R.; Shokri, E. *Turk. J. Chem.* **2017**, *41*, 135-152.
10. Ofomaja, A. E.; Unuabonah, E. I.; Oladoja, N. A. *Bioresour. Technol.* **2010**, *101*, 3844-3852.
11. Al Bsoul, A.; Zeatoun, L.; Abdelhay, A.; Chiha, M. *Desalin. Water Treat.* **2013**, *3994*, 37-41.
12. Nadaroglu, H.; Kalkan, E.; Demir, N. *Desalination* **2010**, *251*, 90-95.
13. Zhang, N.; Zang, G. L.; Shi, C.; Yu, H. Q.; Sheng, G. P. *J. Hazard. Mater.* **2016**, *316*, 11-18.
14. Türker, A. R. *Turk. J. Chem.* **2016**, *40*, 847-867.
15. Al-Qodah, Z.; Al-Shannag, M.; Amro, A.; Assirey, E.; Bob, M.; Bani-Melhem, K.; Alkasrawi, M. *Turk. J. Chem.* **2017**, *41*, 190-208.
16. Langmuir, I. *J. Am. Chem. Soc.* **1918**, *40*, 1361-1403.
17. Freundlich, H. *Z. Phys. Chem.* **1906**, *57*, 385-470.
18. Mahramanlioglu, M.; Kizilcikli, I.; Bicer, I. O. *J. Fluorine Chem.* **2002**, *115*, 41-47.
19. Lagergren, S. *K. Sven. Vetenskapsakad. Handl.* **1898**, *24*, 1-39.

20. Ho, Y. S.; McKay, G. *Process Biochem.* **1999**, *34*, 451-465.
21. Weber, W. J. Jr; Morris, J. C. *J. Sanit. Eng. Div. Proc. Am. Soc. Civ. Eng.* **1963**, *89*, 31-59.
22. Aliyeva, S.; Maharramov, A.; Azizov, A.; Alosmanov, R.; Buniyatzadeh, I.; Eyvazova, G. *Anal. Lett.* **2016**, *49*, 2347-2364.
23. Poots, V. J. P.; McKay, G.; Healy, J. J. *Water Res.* **1976**, *10*, 1061-1066.
24. İşlek Coşkun, Y.; Çiftçi, T. D.; Henden, E. *Desalin. Water Treat.* **2016**, *57*, 20411-20421.
25. Reddy, D. H. K. ; Lee, S. M. *J. Appl. Polym. Sci.* **2013**, *130*, 4542-4550.